AGU PUBLICATIONS

Water Resources Research

RESEARCH ARTICLE
10.1002/2015WR017969

Key Points:
- Definition of potential evaporation using a steady state reference temperature
- Generalization of complementary relationship between actual and potential evaporation
- Physically based estimation of the CR asymmetry parameter (b) and actual evaporation

Correspondence to:
M. Aminzadeh,
milad.aminzadeh@usys.ethz.ch

Citation:
Aminzadeh, M., M. L. Roderick, and D. Or (2016), A generalized complementary relationship between actual and potential evaporation defined by a reference surface temperature, *Water Resour. Res.*, *52*, 385–406, doi:10.1002/2015WR017969.

Received 6 AUG 2015
Accepted 9 DEC 2015
Accepted article online 13 DEC 2015
Published online 22 JAN 2016

A generalized complementary relationship between actual and potential evaporation defined by a reference surface temperature

Milad Aminzadeh[1], Michael L. Roderick[2,3], and Dani Or[1]

[1]Department of Environmental Systems Science, ETH Zürich, Zürich, Switzerland, [2]Research School of Earth Sciences and Research School of Biology, Australian National University, Canberra, Australia, [3]Australian Research Council Centre of Excellence for Climate System Science, Canberra, Australia

Abstract The definition of potential evaporation remains widely debated despite its centrality for hydrologic and climatic models. We employed an analytical pore-scale representation of evaporation from terrestrial surfaces to define potential evaporation using a hypothetical steady state reference temperature that is common to both air and evaporating surface. The feedback between drying land surfaces and overlaying air properties, central in the Bouchet (1963) complementary relationship, is implicitly incorporated in the hypothetical steady state where the sensible heat flux vanishes and the available energy is consumed by evaporation. Evaporation rates predicted based on the steady state reference temperature hypothesis were in good agreement with class A pan evaporation measurements suggesting that evaporation from pans occurs with negligible sensible heat flux. The model facilitates a new generalization of the asymmetric complementary relationship with the asymmetry parameter *b* analytically predicted for a wide range of meteorological conditions with initial tests yielding good agreement between measured and predicted actual evaporation.

1. Introduction

Notwithstanding its centrality to hydrology and climate, the definition and application of the concept of potential evaporation remain heavily debated [*Granger*, 1989; *Nash*, 1989; *Morton*, 1991; *Lhomme*, 1997; *Donohue et al*., 2010; *McMahon et al*., 2013; *Shuttleworth*, 2014; *Milly and Dunne*, 2011]. Potential evaporation is often used to define a reference state for evaporative losses under nonlimiting surface diffusive resistance [*Bateni and Entekhabi*, 2012], or for deducing actual evaporation from measurable meteorological variables or from pan evaporation measurements [*Brutsaert and Stricker*, 1979; *Hobbins et al*., 2001; *Brutsaert*, 2005; *Kahler and Brutsaert*, 2006]. The potential evaporation concept is especially interesting in the framework of the complementary relationship (CR) that links potential evaporation and actual evaporation as postulated by *Bouchet* [1963]. The key idea behind the CR formalism is that as a surface dries, a fraction of the energy not used for evaporation becomes available in the form of increased sensible heat flux [*Brutsaert and Parlange*, 1998; *Brutsaert*, 2005] that increases potential evaporation and gives rise to a complementary relation between actual evaporation and potential evaporation. Such a relation offers a simple and attractive framework for estimating actual evaporation based on calculated potential evaporation (or measured pan evaporation) without detailed knowledge of surface properties.

Implicit to the *Bouchet* hypothesis is a hypothetical evaporation rate around which the symmetric complementary relation forms denoted as E_w "wet environment evaporation" which is the evaporation from an extensive well-watered surface where input energy is the limiting factor. A general form of the CR relation was proposed by *Kahler and Brutsaert* [2006]:

$$(1+b)E_w = bE_a + E_p \tag{1}$$

where b is an empirical constant, and E_a and E_p are actual and potential evaporation, respectively. This form was also implicit in the earlier studies of *Brutsaert and Stricker* [1979], *Brutsaert and Parlange* [1998], and *Brutsaert* [2005]. The symmetric CR hypothesized by Bouchet requires that $b=1$. However, theoretical and experimental evidence shows that b generally exceeds 1 [*Kahler and Brutsaert*, 2006; *Pettijohn and Salvucci*, 2009;

Yang et al., 2013] implying an asymmetric form of the CR. As of yet, it is unclear how and why the parameter *b* varies across systems and conditions.

The objectives of this study are: (1) to provide a new definition of potential and "wet environment" evaporation rates based on steady state surface temperature at which the sensible heat flux vanishes; (2) to use the new formulation of steady state evaporation and analytically generalize the asymmetrical complementary relationship through physically based prediction of *b* parameter; and (3) to estimate actual surface evaporation rates for a range of atmospheric conditions based on predicted *b* parameter and steady state reference evaporation.

Following this introduction, a brief overview of the asymmetric CR is presented. We then present a new formulation that defines a reference state using a hypothetical steady state temperature that is common to both air and evaporating surface. The reference state is obtained by finding the surface-air temperature that satisfies the surface energy balance (SEB) while assuming the vapor concentration of the near-surface air remains constant. With this reference state definition we were able to *a priori* calculate the parameter *b* and use it to estimate actual evaporation through the generalized complementary relationship.

2. Overview of the Asymmetric Complementary Relationship (CR)

2.1. Conceptual Difficulties

Previous investigations of the CR have demonstrated that a symmetric complementary relationship between actual and potential evaporation (i.e., $b=1$ in equation (1)) rarely occurs, and the increase in potential evaporation with surface drying is often higher than the reduction in actual evaporation [*Kahler and Brutsaert*, 2006; *Pettijohn and Salvucci*, 2009; *Yang et al*., 2013]. The asymmetric nature of the CR has been attributed to the definition of potential evaporation and its variation with changes in air characteristics during surface drying [*Brutsaert*, 2005]. Many of the methods used for potential evaporation estimation have evolved from *Penman*'s [1948] combination method (combining energy balance with vapor transfer) that expresses *potential evaporation* from a free water surface as:

$$LE_{Pe}=\frac{\Delta}{\Delta+\gamma}R_n+\frac{\gamma}{\Delta+\gamma}DPA \tag{2}$$

where R_n is the net radiation, γ is the psychrometric constant, Δ is the slope of saturated vapor pressure curve at air temperature, and *DPA* is the drying power of air often characterized by an empirical wind function and vapor pressure deficit. *Monteith* [1965] extended the Penman formulation to include the physiological control by vegetation on the evaporation from leaves and canopies. The Penman-Monteith equation [*Monteith*, 1965] is often used to estimate potential evapotranspiration by measuring real-world meteorological conditions under real-world surface conditions but then arbitrarily assigning the surface resistance to be zero in order to complete the calculations. However, land-atmosphere coupling means that the meteorology is not independent of the surface conditions (i.e., the surface resistance) [Shuttleworth, 2012]. In other words, if the surface resistance was truly zero then the measured meteorology would have been different. One way to address the coupling between surface resistance and meteorological variables using the Penman-Monteith approach equation is to introduce additional resistance(s) such as the climatological resistance [*Shuttleworth et al*., 2009]. That represents a useful approach but here we sought to further investigate the CR using equation (1) as a basis.

Brutsaert [2005] referred to potential evaporation estimated using meteorological data under nonpotential conditions (i.e., when the surface resistance was greater than zero) as the "apparent potential evaporation" (e.g., Penman equation) arguing that interactions between air flow and land surface alter potential evaporation relative to values obtained for a wet surface. The feedback and nature of air-surface interactions require particular attention to the surface wetness and its effect on energy partitioning as a surface gradually dries [*Aminzadeh and Or*, 2014]. Aspects of land-atmosphere coupling were also implicit in Bouchet's original hypothesis, in particular the feedback between declining actual evaporation that modifies air properties and alters potential evaporation relative to the hypothetical condition of the evaporation from an extensive wet environment (E_w). Thus, the definition of reference conditions and variation of potential evaporation in response to the land-atmosphere feedbacks are essential for estimation of actual evaporation based on the complementary relationship.

2.2. Empirical Studies of the CR

Kahler and Brutsaert [2006] have studied how pan evaporation (representative of atmospheric evaporative demand) varies with drying of the surrounding land surface. They proposed a generalized form of the complementary relationship (equation (1)) using an empirical parameter ($b \geq 1$) that accounts for pan evaporation enhancement with the reduction of actual evaporation from the drying land surface, and defined by:

$$b = \frac{E_p - E_w}{E_w - E_a} \tag{3}$$

this definition of parameter b asserts that the increase of potential evaporation (E_p) above the wet environment evaporation (E_w) is proportional to the energy flux that becomes available with surface drying and reduction in evaporation rate. *Pettijohn and Salvucci* [2009] considered variations of potential evaporation with drying of the land surface using 2-D modeling of the interaction between a standard class A evaporation pan and the surrounding environment. They argued that lateral energy and vapor diffusion exchanges of the pan with the surrounding environment are responsible for the asymmetry in the complementary relationship (i.e., $b > 1$) in which a unit variation of actual evaporation is accompanied by approximately five-fold variation of potential evaporation.

Normalization of equation (1) leads to the following expressions for scaled actual evaporation ($E_{a+} = E_a/E_w$) and scaled potential evaporation ($E_{p+} = E_p/E_w$) as functions of the dimensionless moisture index ($E_{MI} = E_a/E_p$):

$$E_{a+} = \frac{(1+b)E_{MI}}{1+bE_{MI}} \tag{4a}$$

$$E_{p+} = \frac{1+b}{1+bE_{MI}} \tag{4b}$$

where E_{MI} is the surface moisture index (with maximum value of 1) indicating how close the landscape is to potential conditions. Figure 1 depicts variations of E_{a+} and E_{p+} as functions of the evaporative moisture index, E_{MI}, for different values of b. The parameterization used in Figure 1 demonstrates that E_{a+} and E_{p+} are less sensitive to variations in b when surfaces are close to saturation, and the main difference emerges for dry surfaces as actual evaporation (E_a) diminishes. At the limit of a completely dry surrounding surface (i.e., $E_a = 0$), the definition of parameter b simplifies to:

$$b = \frac{E_p - E_w}{E_w} \tag{5}$$

this simplification will be used in section 5.2 to clarify the origins of b parameter based on a physically-based framework.

Previous empirical investigations have used pan evaporation data to calibrate b with E_w defined by the *Priestley and Taylor* [1972] estimate [*Kahler and Brutsaert*, 2006]:

$$LE_{P-T} = \alpha_{P-T} \frac{\Delta}{\Delta+\gamma}(R_n - G) \tag{6}$$

where the Priestley-Taylor parameter (α_{P-T}) was determined from local measurements. Additionally, as the surrounding dry surface becomes wetter and actual evaporation increases, surface temperature is expected to decrease as will the outgoing long wave radiation thereby increasing the net radiation. Such adjustments are not accounted for if net radiation under drier (wetter) conditions is assumed to remain constant under wetter (drier) conditions. Hence, it is clear that variations of surface temperature with surface drying (or wetting) must be considered when quantifying wet environment evaporation (E_w) that is central to the CR approach.

2.3. Previous Derivations of the CR

A previous theoretical investigation of the CR has considered, in principle, the possibility of changes in surface temperature with wetting or drying [*Granger*, 1989]. In that study, *Granger* [1989] defined E_a, E_w, and E_p via the corresponding vapor pressure gradients quantified at the relevant (surface) temperatures according to:

$$\partial E = E_w - E_a = f(u)(e_w^* - e_a) - f(u)(e_s - e_a) = f(u)(e_w^* - e_s) \tag{7a}$$

$$\partial E_p = E_p - E_w = f(u)(e_p^* - e_a) - f(u)(e_w^* - e_a) = f(u)(e_p^* - e_w^*) \tag{7b}$$

where $f(u)$ is an empirical wind function, e_a is the air vapor pressure, e_s is the vapor pressure at the drying surface, e_p^* is saturated vapor pressure at surface temperature (T_s) and e_w^* is saturated vapor pressure of a hypothetical wet surface at temperature T_w. Combining equations (7a) and (7b) yields:

$$\frac{E_p - E_w}{E_w - E_a} = \frac{e_p^* - e_w^*}{e_w^* - e_s} \tag{8}$$

Without explicitly invoking the asymmetry b parameter (equation (3)), the relationship expressed in equation (8) implicitly represents this parameter based on vapor pressure gradients for unknown surface temperatures. *Granger* [1989] assumed the net radiation is constant as the surface wetness changes which implies that the change in sensible heat flux (H) was of equal and opposite sign to the change of latent heat flux (LE), leading to the relation:

$$\frac{\partial H}{\partial LE} = -1 = \gamma \frac{T_w - T_s}{e_w^* - e_s} \tag{9}$$

However, as noted above, and elsewhere [*Aminzadeh and Or*, 2013], the surface temperature does change during surface drying or wetting which, in turn, changes the net radiation and limits the applicability of equation (9). The critical role of surface temperature variation with surface drying in definition of b parameter based on equation (8) will be presented in section 5.2.

Combining equations (8) and (9) results in the asymmetrical complementary relationship as:

$$\left(1 + \frac{\Delta^*}{\gamma}\right) E_w = \frac{\Delta^*}{\gamma} E_a + E_p \tag{10}$$

An important point in derivation of equation (10) through equations (7)–(9) is the definition of Δ^* using the (unknown at this stage) surface temperatures as:

$$\Delta^* = \frac{(e_p^* - e_w^*)}{(T_s - T_w)} \tag{11}$$

Although *Granger* [1989] provided an unambiguous definition of Δ^* in this context, some researchers have interpreted it as the slope of saturated vapor pressure at air temperature [e.g., *Venturini et al.*, 2012]. The crucial point here is that Δ^* is defined using two unknowns, the drying surface temperature (T_s) and the hypothetical wet surface temperature (T_w) and both must be specified in this version of the asymmetrical complementary relationship. A similar relationship representing the "b" parameter in equation (1) as $b = \Delta^*/\gamma$ (see equation (10)) was proposed by *Szilagyi* [2007] considering Δ^* as an effective slope of the saturation vapor pressure curve. In the absence of surface temperatures (T_s and T_w) for quantifying Δ^*, *Szilagyi* [2007] proposed an empirical correction coefficient, ε, to express $\Delta^* = \varepsilon\Delta$ in which Δ is quantified based on air

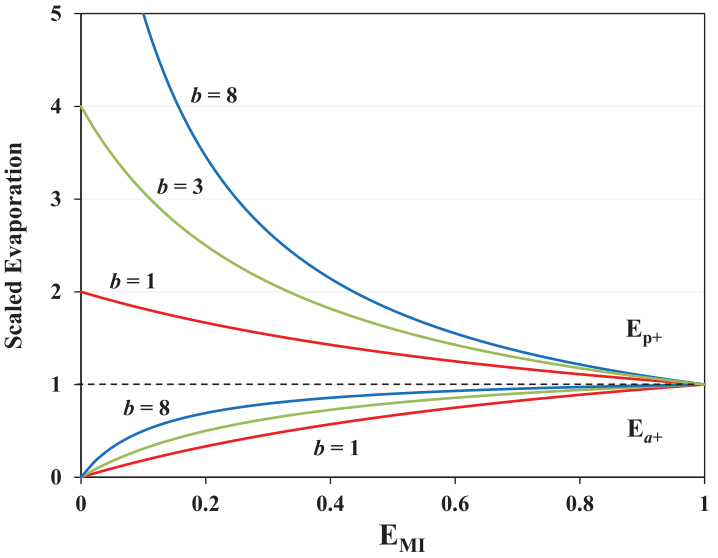

Figure 1. $E_{a+} = E_a/E_w$ and $E_{p+} = E_p/E_w$, as functions of the evaporative moisture index $E_{MI} = E_a/E_p$. The curves were obtained with equations (4a) and (4b), respectively, for different values of the effectiveness parameter, b [*Kahler and Brutsaert*, 2006].

temperature. The correction parameter ε is determined through a calibration process, and in some cases it has been tacitly assumed to be unity [*Yang et al*., 2013].

In summary, there is broad consensus supported by limited experimental evidence regarding some sort of complementarity between actual and potential evaporation as a surface dries. Presently, the definitions of potential evaporation as a reference state using meteorological variables (for the complementary relationship) are critically dependent on assumptions regarding aerodynamic effects in Penman's equation [*Brutsaert and Stricker*, 1979; *Granger*, 1989]; on locally calibrated coefficients [*Priestley and Taylor*, 1972]; or on generally unavailable surface temperature for prediction of energy partitioning and quantification of vapor pressure deficit [*Granger*, 1989; *Crago and Crowley*, 2005; *Szilagyi*, 2007]. Moreover, the wet environment evaporation (E_w) serves as a reference state in the complementary relationship, yet, it has often been quantified based on the meteorological data obtained under nonwet conditions (e.g., using P-T equation) [*Brutsaert and Stricker*, 1979], or unknown surface temperatures [*Granger*, 1989]. Consequently, the general form of the complementary relationship and estimation of actual evaporation from the CR approach remain ambiguous.

2.4. A New Reference Surface Temperature-Based Approach to the CR

We propose a new framework for the CR that explicitly resolves the surface temperature of a drying surface (T_s) and defines a hypothetical wet surface temperature (T_w) thereby allowing for consistent estimates of the net radiation and air properties as a surface wets or dries. The new formulation employs a surface element centered around an evaporating pore (i.e., a pore-scale representation) and directly links surface energy balance components including surface resistance due to pore-scale diffusive interactions [*Aminzadeh and Or*, 2014]. We then postulate a hypothetical steady state condition where the drying surface and the air reach a common equilibrium temperature. This state implicitly considers complete air-surface feedback that concurrently adjusts surface and air temperatures to a common reference temperature while a surface wets/dries. Evaporation from a small saturated surface surrounded by a large drying region represents potential evaporation in our model. Accordingly, the hypothetical reference temperature is used to quantify wet environment evaporation (i.e., the evaporation from an extensive wet surface) and the subsequent variation of potential evaporation with changes in surface water content during surface drying. The theoretical background of the steady state surface temperature and model derivation of potential evaporation are presented in the following section.

3. Theoretical Considerations

3.1. Steady State Surface Temperature for Potential Evaporation

We propose a physically based approach for prediction of potential evaporation through explicit calculation of surface energy balance components including long wave radiation and soil heat flux. A closed land-atmosphere system with negligible dry air entrainment at the top of the convective boundary layer (CBL) is assumed [*McNaughton*, 1976; *Perrier*, 1980; *Raupach*, 2001] to investigate surface energy balance and feedback processes between surface and air flow that is also similar to the closed-box model [*Lhomme*, 1997]. Energy exchange across the system boundaries occurs via radiation and soil heat flux. Hence, the net available energy within the system is partitioned between evaporative and sensible heat fluxes:

$$(1-\alpha)R_S+R_{L,in}-R_{L,out}-G=H+LE_a \tag{12a}$$

where α is the surface albedo, R_S is the incoming shortwave radiation flux while $R_{L,in}$ and $R_{L,out}$ are incoming and outgoing long wave radiation, respectively, and G is soil heat flux. The first term on the left hand side of equation (12a) represents the net shortwave radiation at the surface denoted as $R_{S,net}$. We use theory developed previously based on a pore-scale representation of coupled mass and energy exchange over evaporating and drying porous surfaces to explicitly describe each of the energy fluxes in equation (12a) [*Aminzadeh and Or*, 2013] (Figure 2). That theory enables consideration of dynamic effects of water availability on energy partitioning and surface heat fluxes. The formulation considers intrinsic resistance to vapor diffusion from drying surfaces [*Schlünder*, 1988; *Haghighi et al*., 2013; *Haghighi and Or*, 2015] with the SEB for a surface unit cell (with an evaporating pore at its center) written as:

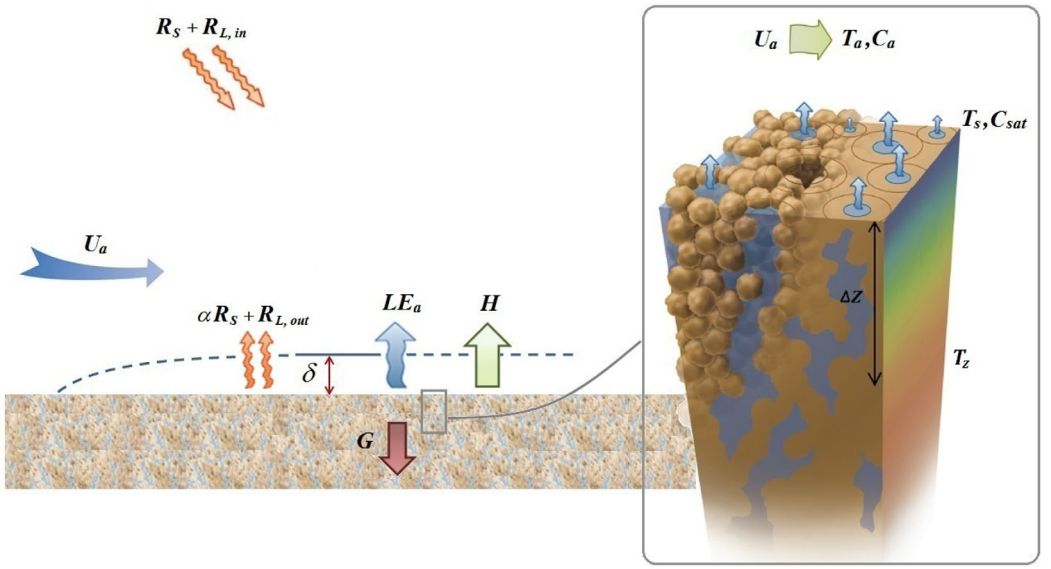

Figure 2. Schematic sketch of an evaporating porous medium with surface energy balance components and a surface overlain by unit cells centered on an evaporating pore (for details, see *Aminzadeh and Or* [2014]). The reduction of surface water content during surface drying is represented by an increase in the dry region around individual wet pores on the surface (brown circles).

$$(1-\alpha)R_S+\sigma\varepsilon_a T_a^4-\sigma\varepsilon_s T_s^4-\frac{k}{\Delta Z}(T_s-T_Z)=h_a(T_s-T_a)+\frac{D_a\lambda[C_{sat}(T_s)-C_a]}{\delta(1+\Phi)} \tag{12b}$$

in which Schlünder's diffusive resistance parameter Φ is defined as:

$$\Phi=\frac{2a}{\pi\delta}\sqrt{\frac{\pi}{4\theta}}\left[\sqrt{\frac{\pi}{4\theta}}-1\right] \tag{12c}$$

where ε_s and ε_a are surface and atmospheric emissivity, respectively, a is the characteristic pore size, δ is the boundary layer thickness that is characterized using the wind speed (U_a) [*Haghighi and Or*, 2013], θ is the mean surface water content, D_a is the vapor diffusion coefficient in air, h_a is the air convection heat transfer coefficient, T_a is the air temperature and T_Z is the linearized soil temperature at thermal decay depth (ΔZ) beneath the evaporating surface [*Shahraeeni and Or*, 2011; *Aminzadeh and Or*, 2014]. In equation (12b), C_{sat} represents saturated vapor concentration at the surface of unit cell's evaporating pore and C_a is the vapor concentration within the air mass (characterized based on air temperature and relative humidity) interacting with drying surface, which, alternatively, could be expressed in terms of specific humidity.

While in real conditions the CBL may grow and entrain drier and warmer air from the free atmosphere, the concept of closed land-atmosphere system has been used by *McNaughton* [1976], *Perrier* [1980], and *Lhomme* [1997] to characterize land-atmosphere feedbacks showing that the effect of entrainment on evaporation dynamics is relatively weak. Accordingly, this is the starting point for theoretical analyses in this study enabling considerations of feedbacks between surface and air temperatures that impact sensible heat flux and air warming feedbacks as the surface wets or dries (Figure 3). We seek conditions for estimating potential evaporation described by *Raupach* [2001] as "*the long-term limit of evaporation into a closed system supplied steadily with energy*." We set the upper limit of evaporation where the sensible heat flux is zero ($H=0$), and the system will therefore attain a hypothetical reference temperature such that the temperature of the evaporating (drying) surface is equal to that of the air (Appendix A):

$$T_s=T_a=T_{ss} \tag{13}$$

we define this as the "steady state temperature" (T_{ss}) under the hypothetical imposed condition where most of the available energy drives the latent heat flux (a small amount goes to soil heat flux and adjusts long wave radiation). Hence, for a surface building block composed of an evaporating pore surrounded by dry surface (Figure 2) the resulting coupled energy balance (equation 12) can be expressed explicitly in terms of T_{ss} as:

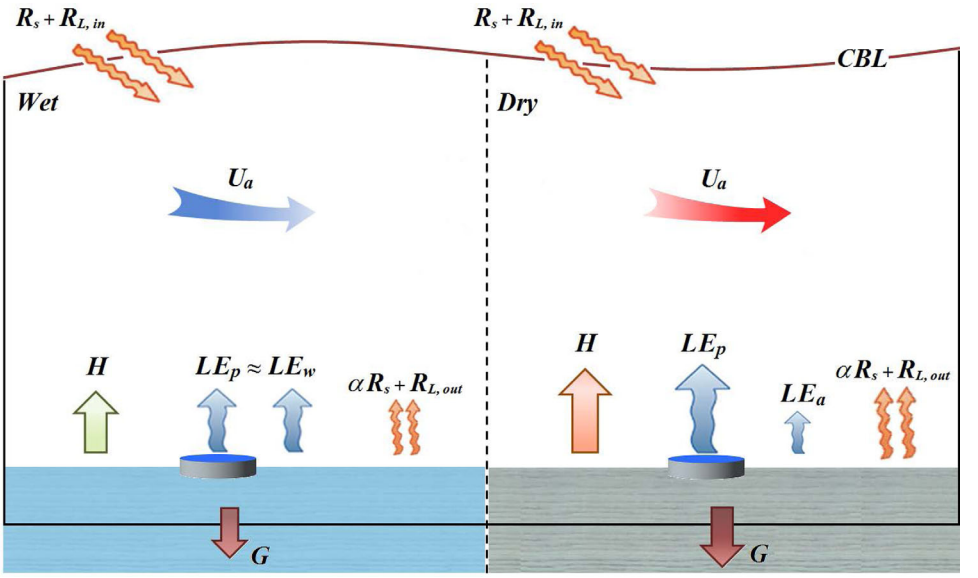

Figure 3. Conceptual diagram showing the effect of feedback process between overlying air flow and land surface on the variation of actual and potential evaporation during surface drying (CBL stands for the convective boundary layer whose vertical dimension may vary with time).

$$(1-\alpha)R_S+\sigma T_{ss}^4(\varepsilon_a-\varepsilon_s)-\frac{k}{\Delta Z}(T_{ss}-T_Z)=\frac{D_a\lambda[C_{sat}(T_{ss})-C_a]}{\delta(1+\Phi)} \tag{14}$$

We further assume that the mean vapor concentration in the near-surface air mass (C_a) remains constant while the system is brought to the imposed condition and that evaporation from the drying land surface does not modify the air column's specific humidity significantly [*McNaughton and Spriggs*, 1989]. The only unknown in equation (14) is the steady state temperature; a solution (root finding) thus yields the value of T_{ss} during surface evaporation for the assumed condition of $H=0$.

3.2. Estimation of Reference Evaporation Based on Steady State Surface Temperature

We consider evaporation from a saturated surface with no surface resistance, and follow *Lhomme*'s [1997] definition of potential evaporation as "*the evaporation that would occur from a hypothetical saturated surface, with radiative properties similar to those of the whole area and small enough that the excess moisture flux does not modify the characteristics of the convective boundary layer*." The steady state reference temperature provides a link between components of the surface energy balance at this hypothetical steady state condition. In addition, we made the assumption of zero sensible heat flux that defines a particular state of feedbacks between the surface and the air as described by equation (14). Accordingly, we consider a small saturated surface surrounded by a large drying region, and evaporation from this saturated surface (e.g., a pan) represents the resulting potential evaporation expressed as diffusive vapor transfer across air boundary layer of thickness δ at the steady state surface temperature [*Machin*, 1970; *Hisatake et al.*, 1995; *Lim et al.*, 2012; *Haghighi and Or*, 2013] as:

$$LE_R(T_{ss})=\frac{D_a\lambda}{\delta}[C_{sat}(T_{ss})-C_a] \tag{15}$$

The steady state reference evaporation (E_R, equation (15)) is used to represent effects of the drying land surface on potential evaporation (E_p) through effects of land-atmosphere feedback process on steady state surface temperature and saturated vapor pressure. Note the language in many of the complementary relationships is "small potential evaporation surface" where the dimension is not really important as long as the evaporation from the small wet surface does not appreciably alter the characteristics of the overlying air.

Estimation of potential evaporation based on an equilibrium surface temperature has been previously proposed by *Morton* [1983] who considered equality between steady state surface energy balance (neglecting

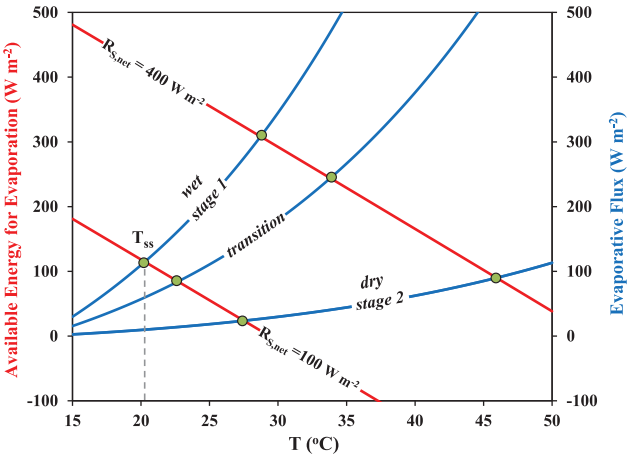

Figure 4. Solution for steady state temperature at three different evaporative regimes as stage 1, transition, and stage 2 assuming U_a=1 m s^{-1}, ε_s=0.9, ε_a=0.8, T_a=25°C, C_a=0.011 kg m^{-3} (rh=50%), k=1 W m^{-1} K^{-1}, T_Z=25°C, and ΔZ=0.1 m. The left and right vertical axes depict variations of the available energy for evaporation (LHS of equation (14)) and aerodynamic representation of evaporative flux (RHS of equation (14)) with temperature, respectively. The wet and dry surface conditions are marked as different stages of surface evaporation. The intersections of the curves (symbols) show unique values of steady state surface temperature, T_{ss}, for the given radiative and evaporation regimes.

soil heat flux) and aerodynamic vapor transfer for evaporation from a wet surface. A similar definition of equilibrium temperature has been proposed by *Edinger et al*. [1968] as the surface temperature at which the net rate of energy exchange over water surfaces is zero. Accordingly, the resulting equilibrium surface temperature has been used to quantify components of surface energy balance (net radiation and sensible heat flux) and calculate potential evaporation as the residual of SEB over moist surfaces [*Morton*, 1983]. Note that our definition of potential evaporation presented in equation (15) should not be confused with either the equilibrium temperature potential evaporation of *Morton* [1983], or the equilibrium evaporation of *Slatyer and McIlroy* [1961]. A definitive review of the various forms of equilibrium evaporation is provided in *Raupach* [2001].

4. Methods and Materials

4.1. Reference Surface Temperature (T_{ss}) and Steady State Evaporation (E_R)

The left hand side (LHS) of equation (14) represents the available energy for evaporation including net radiation and soil heat flux, while the right hand side (RHS) is the aerodynamic representation of the evaporative flux (at a hypothetical steady state with zero sensible heat flux). Figure 4 illustrates variations of LHS and RHS of equation (14) with temperature for different values of net shortwave radiation during stage 1 evaporation, transition to stage 2, and at stage 2 evaporation. The increase in surface temperature increases outgoing long wave radiation and soil heat flux that, in turn, decreases the LHS for a constant net shortwave radiation flux. On the other hand, increased surface temperature enhances evaporative flux by increasing the vapor pressure gradient for a constant surface wetness. The intersections of the curves (marked by symbols) in Figure 4 depict unique values where the energetic (LHS) and aerodynamic (RHS) representation of evaporative flux are equal and yield a specific steady state surface temperature, T_{ss}, that fulfills the condition of zero sensible heat flux as per the original definition (equation (14)). Note that details of the variation of LHS and RHS functions with surface temperature are not central to this analysis, only their intersection.

To compare model predictions of the reference evaporation based on steady state surface temperature (equation (15)) with widely used measures, we compare $E_R(T_{ss})$ with the PenPan [*Rotstayn et al*., 2006], Penman (equation (2)), and Priestly-Taylor (equation (6)) estimates. The PenPan model is a generalized form of the Penman's equation that has been designed and calibrated to represent class A pan evaporation. The radiative and aerodynamic components in PenPan are calculated based on *Linacre* [1994] and *Thom et al*. [1981], respectively (for details, see *Rotstayn et al*. [2006] and *Roderick et al*. [2007]). For further tests of the model we also compare $E_R(T_{ss})$ with monthly average pan evaporation made at Tucson and Yuma (Arizona), and Grand Junction (Colorado) where associated meteorological data [*Western Regional Climate Center*, 2014; *Jensen and Haise*, 1963] needed for evaluation of the model were available.

4.2. Physically Based Prediction of the *b* Parameter

Generalization of complementary relationship proposed by *Kahler and Brutsaert* [2006] remains widely empirical with parameter b quantified through the measurements. We aim to analytically predict variation of b parameter represented in equation (3) using a physically based framework that employs the steady state reference evaporation for quantification of potential and wet environment evaporation. The model

Table 1. Characteristics of Experimental Data Used for Evaluation of Equation (16)

Field	Julian Day	Year	Data
Simcoe (Ontario, Canada)	163-168-169-174-181-203-204	1971	*Davies and Allen* [1973], *Environment Canada* [2014]
Station 40 (FIFE project), Konza Prairie (Kansas, USA)	166-177-184-190-246	1987	*Sellers et al.* [1992], *Fritschen* [1994], *Kanemasu* [1994]
Davis (California, USA)	257-271-279-286-297	1990	*Katul and Parlange* [1992]
Site WC23 (SMACEX02), Walnut Creek watershed (Iowa, USA)	182-185-187	2002	*Jackson* [2003], *Jackson and Cosh* [2003], *Prueger et al.* [2009]

predicted b parameter is evaluated using actual and pan evaporation data obtained from measurements in Kansas, USA (Konza Prairie and Tuttle Creek Reservoir) [*Kahler and Brutsaert*, 2006], and in Walnut Creek watershed (Iowa, USA) [*Yang et al.*, 2013]. For data from Kansas we use average meteorological inputs as $R_{S,net}$=310 W m^{-2}, U_a=3 m s^{-1}, T_a=22°C, C_a=0.011 kg m^{-3} obtained from day-time (06:00 to 18:00 CST) averages of half-hourly measurements at stations 40 (May–October 1987) and 944 (July and August 1989) [*Fritschen*, 1994]; and for Walnut Creek watershed the mean meteorological data (10:00 to 16:00 CST) are obtained based on measurements from 16 June to 9 July 2002, at site WC13 as $R_{S,net}$=550 W m^{-2}, U_a=3.6 m s^{-1}, T_a=30.8°C, C_a=0.017 kg m^{-3} [*Jackson and Cosh*, 2003; *Prueger et al.*, 2009].

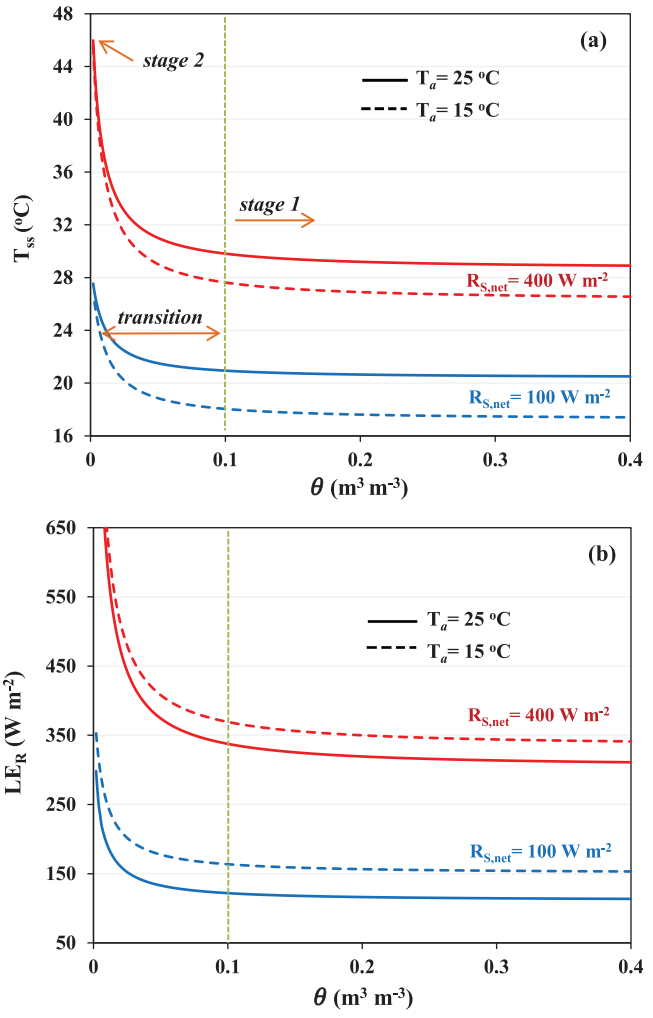

Figure 5. Dependence of (a) steady state reference temperature and (b) $LE_R(T_{ss})$ on the surface wetness. Results were obtained for different values of net shortwave radiation and initial air temperature assuming U_a=1 m s^{-1}, ε_s=0.9 and ε_a=0.8, k=1 W m^{-1} K^{-1}, T_Z=25°C, and ΔZ=0.1 m. Different stages of surface evaporation are characterized based on surface wetness. The value of C_a was quantified for rh=50%.

4.3. Estimation of Actual Evaporation Through the Generalized CR

The most important utility of predicted parameter "b" would be estimation of actual evaporation based on the asymmetrical complementary relationship defined by rearrangement of equation (1) to give:

$$E_a = \frac{(1+b)E_w - E_p}{b} \qquad (16)$$

We employ analytical derivation of b parameter to estimate actual evaporation through the CR framework (equation (16)) in which potential and wet environment evaporations are quantified based on the steady state reference evaporation. The actual evaporation obtained from the newly derived b parameter and reference evaporation is evaluated with field evaporation data. We have used the experimental data of *Davies and Allen* [1973] obtained from measurements at Simcoe in Ontario, the FIFE project at Konza Prairie (station 40) [*Sellers et al.*, 1992; *Fritschen*, 1994; *Kanemasu*, 1994], the SMACEX experiments conducted in Walnut Creek watershed

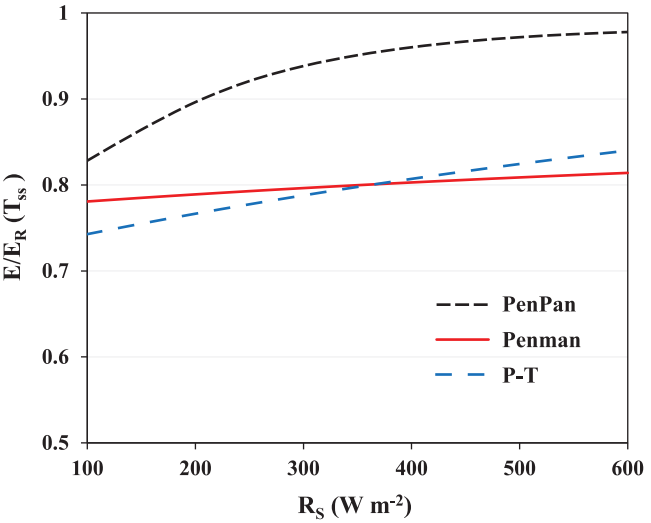

Figure 6. Normalized values of the PenPan, Penman and P-T equations with $E_R(T_{ss})$ versus shortwave radiation obtained based on the surface water content of 0.2 $m^3\ m^{-3}$, rh=50%, T_a=25°C, U_a=2 m s^{-1}, ε_s=0.9, ε_a=0.8, pan albedo of 0.15, and soil albedo of 0.25. The commonly applied class A pan evaporation coefficient (0.7–0.8) is evident in the values of Penman and P-T models.

(Iowa, USA) [*Jackson*, 2003; *Jackson and Cosh*, 2003; *Prueger et al.*, 2009], and lysimeter evaporation data of *Katul and Parlange* [1992] obtained from measurements in Davis, USA. Summary and some details of experimental data are briefly presented in Table 1.

In the following section, we present dynamics of steady state evaporation and analytical prediction of b parameter which are employed to estimate actual evaporation using the generalized complementary relationship.

5. Results and Discussion

5.1. Dynamics of Steady State Evaporation at Reference Surface Temperature $LE_R(T_{ss})$

The evolutions of the reference temperature (T_{ss}) and associated steady state evaporation at the reference surface temperature (i.e., $LE_R(T_{ss})$ as the representative of potential evaporation) as functions of the surface moisture are illustrated in Figure 5 for different values of initial air temperature and shortwave radiation flux. The nearly constant evaporative flux during stage 1 evaporation is the result of complex micro-adjustments of vapor diffusion exchange through the air boundary layer [*Shahraeeni et al.*, 2012] that yield a nearly constant steady state temperature for a wide range of surface water contents. The subsequent large reduction in evaporative flux at the end of stage 1 evaporation (transition to stage 2) [*Monteith*, 1981; *Aminzadeh and Or*, 2014] results in changes in energy partitioning. The excess energy not able to be used for evaporation as the surface dries, manifests itself as an increase in the sensible heat flux associated with an increase in the hypothetical steady state temperature (Figure 5a). Note that the value of vapor concentration in air (C_a) is held constant during surface drying while the air relative humidity (rh) will vary with changes in T_{ss}. These changes are consistent with the notion of drier and warmer air as the surface dries as postulated in the earlier concepts that underpin the complementary relationship [*Bouchet*, 1963; *Brutsaert and Stricker*, 1979].

Figure 5b depicts variations in $LE_R(T_{ss})$ with surface drying obtained from equation (15) corresponding to T_{ss} in Figure 5a. The differences in the resulting LE_R values with surface drying illustrate that a symmetrical complementary relationship as postulated by *Bouchet* [1963] is not common. Notwithstanding the similarity between the present model and the analysis of *Pettijohn and Salvucci* [2009] for enhancement of potential evaporation with surface drying we note the underlying physical reasons are different. The increase of $LE_R(T_{ss})$ with surface drying as reported here (Figure 5b) is the result of an increase of T_{ss} that is inferred from the condition of zero sensible heat flux over the drying surface, whereas the increase of potential evaporation in *Pettijohn and Salvucci* [2009] with surface drying was attributed to negative sensible heat flux toward the pan.

To assess model predictions of the reference evaporation based on the steady state surface temperature concept (equation (15)) we plotted potential evaporation predictions by the PenPan, Penman, and P-T equations normalized by estimates of $E_R(T_{ss})$ as a function of the incoming shortwave radiation in Figure 6. Potential evaporation predictions by Penman and P-T equations are typically lower than $E_R(T_{ss})$ by about 20% to 30%. That is anticipated because our reference surface assumes no sensible heat flux, while the saturated surfaces studied by *Priestley and Taylor* [1972, Figure 2] have a Bowen ratio of around 0.3 which accounts for the above-noted differences.

Natural evaporating surfaces at steady state temperature (with H=0) are probably rare; however, measurements show that evaporation from class A pans often occurs with near-zero sensible heat flux, especially during summer [*Lim et al.*, 2013]. Those observations would also explain the close agreement of $E_R(T_{ss})$ with PenPan estimates (black dashed-line in Figure 6) under typical sunny conditions (e.g., $R_S > 400$ W m^{-2}).

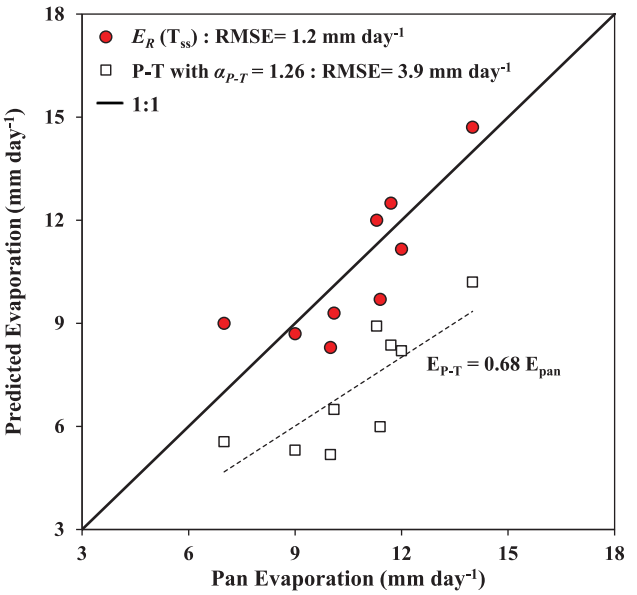

Figure 7. Comparison between values of $E_R(T_{ss})$ obtained from equation (15) with monthly average pan evaporation for Tucson (May, June, July, August, September, October), Yuma (July, August), and Grand Junction (August) [*Western Regional Climate Center*, 2014] assuming surface water content of 0.2 m^3 m^{-3} for the surrounding land. Squares depict comparison between pan data and estimations of wet surface evaporation using the P-T relation obtained with $\alpha_{P-T}=1.26$. The regression line with slope of 0.68 for P-T estimations follows the pan coefficient. The radiation fluxes were estimated from *Jensen and Haise* [1963].

We sought further tests of the approach and have also compared $E_R(T_{ss})$ with both pan evaporation measurements and Priestly-Taylor estimates of evaporation (Figure 7). We calculated E_{P-T} (equation (6)) and $E_R(T_{ss})$ (equation (15)) and compared the results with the pan evaporation measurements conducted in Arizona and Colorado, USA [*Western Regional Climate Center*, 2014]. Model estimates of steady state reference evaporation show good agreement with pan evaporation data. The widely used E_{P-T} (with $\alpha_{P-T}=1.26$) was only around 68% of the pan evaporation and consistent with typical values of the pan coefficient (~0.7–0.8).

5.2. The Origins of the Asymmetrical Parameter *b* and its Physically Based Prediction

The agreement between model predictions of potential evaporation and pan evaporation measurements motivated application of the model to describe the asymmetrical complementary relationship. We seek to develop a physically based estimation of the efficiency parameter "*b*" of *Kahler and Brutsaert* [2006] by using steady state reference evaporation ($E_R(T_{ss})$) to estimate potential and wet environment evaporation in equation (3) as:

$$b_{ss}=\frac{E_R(T_{ss})-E_w(T_{ss})}{E_w(T_{ss})-E_a(T_s)} \tag{17}$$

The physically based prediction of *b* parameter based on T_{ss} and $E_R(T_{ss})$ is hereby denoted as b_{ss} to differentiate it from the *b* parameter that is deduced from measured evaporation data [*Kahler and Brutsaert*, 2006]. The various terms can be readily plotted on a standard temperature-vapor concentration curve (Figure 8). Accordingly, the parameter b_{ss} can be expressed as:

$$b_{ss}=\frac{\frac{D_a}{\delta}\left(C_{sat}(T_{ss}|_{\theta})-C_a\right)-\frac{D_a}{\delta}\left(C_{sat}(T_{ss}|_{\theta_{sat}})-C_a\right)}{\frac{D_a}{\delta}\left(C_{sat}(T_{ss}|_{\theta_{sat}})-C_a\right)-\frac{D_a}{\delta(1+\Phi)}\left(C_{sat}(T_s|_{\theta})-C_a\right)}=\frac{z-x}{x-\frac{y}{1+\Phi}} \tag{18}$$

where T_s is the surface temperature, T_{ss} is the steady state surface temperature and Φ represents vapor diffusion resistance parameter (equation (12c)).

The extent of the T_{ss} on the horizontal axis of Figure 8 between saturation and dry conditions (θ_{sat} and $\theta=0$) reflects the properties of the drying surface and places the system at different locations of temperature-vapor pressure relations thereby defining the value of b_{ss} with atmospheric inputs. The variation of actual evaporation ($\frac{y}{1+\Phi}$) and potential evaporation (z) with respect to the (constant) wet environment evaporation (*x*) is captured by the constant b_{ss} for the entire range of surface moisture content. The representation in equation (18) is similar to the interpretation of *Granger* [1989] expressed here in equation (8). The essential difference is that the approach proposed here allows estimation of the appropriate surface temperature that is essential for prediction of this important CR asymmetry parameter (*b*).

Assuming that the value of *b* is constant for the entire range of surface moisture content, we employ equation (5) that is the simplified form of equation (3) for dry condition where $E_a=0$ (i.e., $\frac{y}{1+\Phi}=0$) to analytically

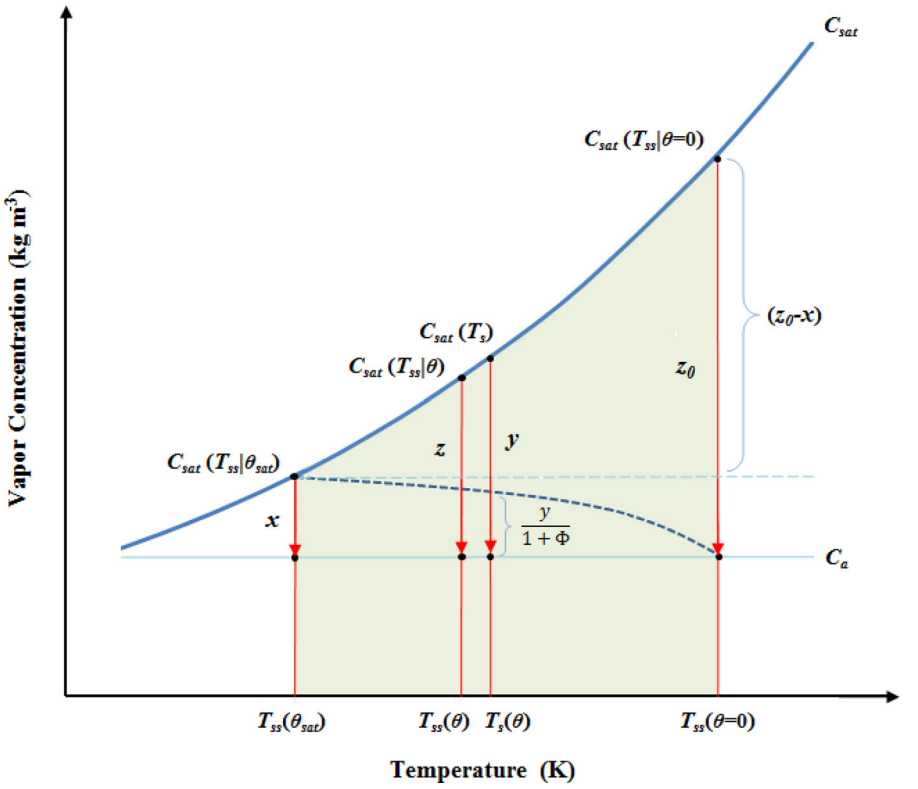

Figure 8. Schematic representation of variation of actual, potential and wet environment evaporation depicted as $\frac{y}{1+\Phi}$ (thick dashed-line), z, and x, respectively, during surface drying. The parameter z_0 represents reference evaporation for dry condition. The saturation vapor concentration curve (C_{sat}) was obtained from the Clausius-Clapeyron relation. The range of steady state temperature on horizontal axis is related to the properties of the drying surface and the atmospheric inputs, and it reflects the origins of the CR asymmetry and how b_{ss} varies with surface properties (affecting the range of temperature increase) and atmospheric inputs (the position of green shaded area).

predict the value of b parameter for various atmospheric inputs. The values of potential and wet environment evaporation are then calculated using model estimates of reference evaporation (E_R in equation (15)) and based on the steady state reference temperature (T_{ss}) obtained from equation (14) for wet and dry conditions to quantify E_w and E_p, respectively, for given atmospheric data such that:

$$b_{ss}=\frac{\left(C_{sat}(T_{ss}|_{\theta=0})-C_a\right)-\left(C_{sat}(T_{ss}|_{\theta_{sat}})-C_a\right)}{\left(C_{sat}(T_{ss}|_{\theta_{sat}})-C_a\right)}=\frac{z_0-x}{x} \tag{19}$$

Figure 9 depicts the range of variations of b_{ss} values from equation (19) over a large range of differences in T_{ss} between saturated (θ_{sat}) and completely dry (θ=0) surface conditions. The range of differences in T_{ss} (schematically marked by green shaded area in Figure 8) varies with atmospheric conditions (radiation, wind speed, air vapor concentration). The gray dashed lines in Figure 9 show how b_{ss} and steady state surface temperature difference vary with input radiative flux for a constant wind speed across three values of air vapor concentrations. A crucial point that differentiates this study from *Granger* [1989] and others, is the direct prediction of the corresponding surface temperatures that, in turn, enables closure of the energy balance and latent heat fluxes and permits analytical prediction of the b parameter.

The parameter b_{ss} based on equation (19) was evaluated using experimental data depicted in Figure 10. The results make used of actual and pan evaporation measurements from Kansas, USA, expressed in normalized forms ($E_{a+}=E_a/E_w$ and $E_{p+}=E_p/E_w$) as functions of moisture index ($E_{MI}=E_a/E_p$) [*Kahler and Brutsaert*, 2006]. The solid lines in Figure 10 depict the variations of E_{a+} and E_{p+} versus E_{MI} (equations (4a) and (4b)) with b=4.33 yielding the best fit to measured data in the study by *Kahler and Brutsaert* [2006]. For the meteorological inputs of stations 40 and 944 in Konza Prairie [*Fritschen*, 1994], equation (19) was used to

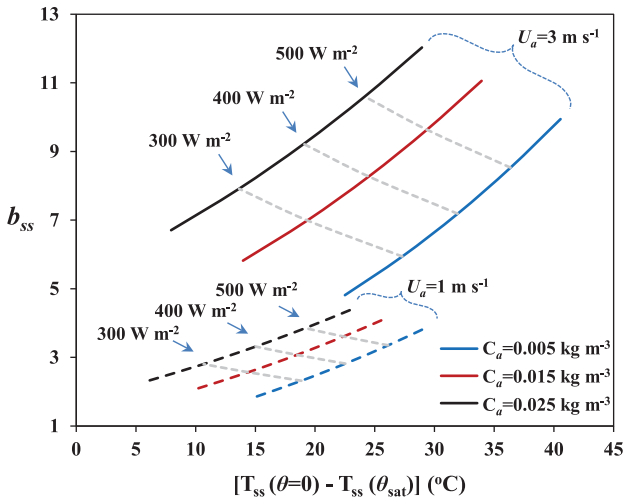

Figure 9. Variation of b_{ss} versus the difference between steady state surface temperature at dry and wet condition. The dashed and solid colored lines represent variations in b_{ss} and steady state temperature difference for constant wind speeds of 1 and 3 m s^{-1}, respectively, and constant vapor concentrations. The gray dashed lines mark constant (shortwave) radiative fluxes ($R_{S,net}$).

predict b_{ss} (dashed lines in Figure 10). We emphasize that the parameter b_{ss} was obtained directly from input meteorological data and not from curve fitting to experimental evaporation results.

Next, we employed equation (19) to systematically extend a physically based prediction of b parameter based on reference evaporation (equation (15)) calculated for a range of atmospheric conditions. The correlation based estimate of b_{ss} driven by atmospheric inputs is denoted as b^*_{ss}. The expressions in equation (20) were obtained as a function of net shortwave radiation, wind speed and air vapor concentration across a range of conditions (see Appendix B):

$$b^*_{ss}=A\,R_{S,net}+B \tag{20a}$$

where $R_{S,net}$ is the net shortwave radiation flux ($(1-\alpha)R_S$ (W m^{-2})) and the parameter A is a function of wind speed (U_a (m s^{-1})):

$$A=(3U_a+2)\times10^{-3} \tag{20b}$$

The parameter B is also determined as function of wind speed (U_a (m s^{-1})) and vapor concentration (C_a (kg m^{-3})) as:

$$B=(24.3U_a-1.44)(C_a+22\times10^{-3})+0.3 \tag{20c}$$

We tested physically-based expression in equation (20) using measurements from the Walnut Creek watershed (Iowa, USA) [*Yang et al.*, 2013] (Figure 11). Relevant meteorological data from the Soil Moisture-Atmosphere Coupling Experiment (SMACEX02) conducted in Walnut Creek [*Jackson and Cosh*, 2003; *Prueger et al.*, 2009] were used to calculate b^*_{ss}. The solid curves in Figure 11 have been obtained using b^*_{ss}= 10.7 and compared with normalized measurements (our estimate of b^*_{ss} was calculated a priori using equation (20) and was not the result of curve fitting).

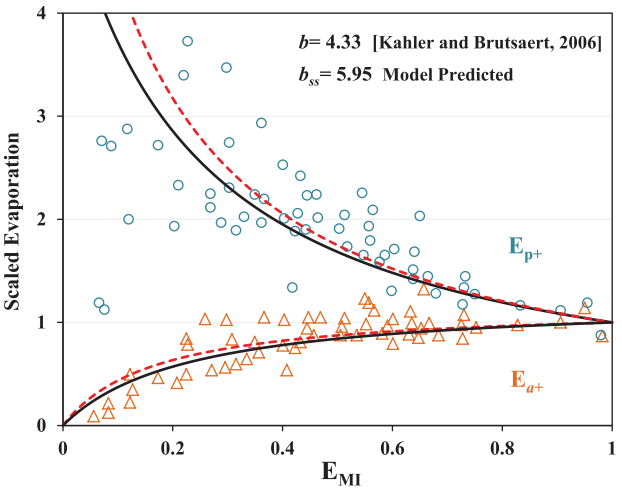

Figure 10. Normalized evaporation data from Kansas and parameterized curves (solid curves) with b=4.33 [*Kahler and Brutsaert*, 2006]. The dashed curves depict the model predicted b_{ss} parameter obtained for day-time (06:00 to 18:00 CST) with average meteorological inputs [*Fritschen*, 1994]: $R_{S,net}$=310 W m^{-2}, U_a=3 m s^{-1}, T_a=22°C, C_a=0.011 kg m^{-3} (rh=60%), assuming ε_s=0.9 and ε_a=0.8.

5.3. Estimation of Actual Evaporation (E_a)

Physically-based prediction of the b parameter highlights applicability of the generalized complementary relationship proposed by *Kahler and Brutsaert* [2006] for estimation of actual evaporation. We evaluated the procedure of estimating actual evaporation through the generalized CR with our derivation of b parameter and reference evaporation by comparing measured (actual) evaporation

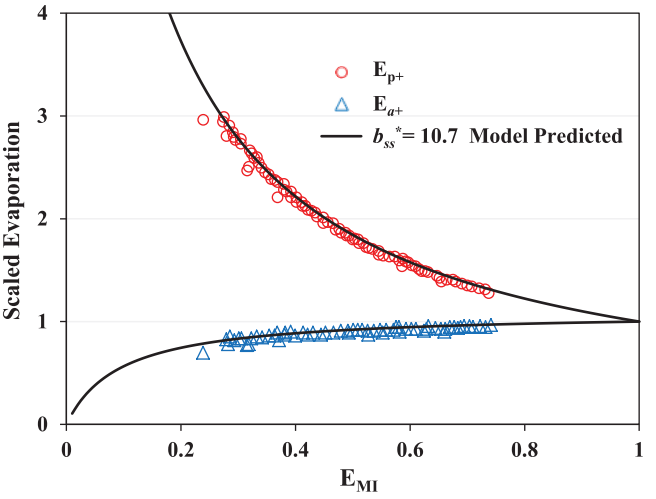

Figure 11. Normalized evaporation data from Walnut Creek (symbols)–site: WC13 [*Yang et al.*, 2013]. The solid curves depict model predicted b parameter (b_{ss}^* from equation (20)) obtained based on mean values of reported meteorological data [*Jackson and Cosh*, 2003; *Prueger et al.*, 2009]: $R_{S,net}$=550 W m^{-2}, U_a=3.6 m s^{-1}, T_a=30.8°C, C_a=0.017 kg m^{-3} (rh=55%).

with predictions based on equation (16). Figure 12 depicts comparison between values of actual evaporation obtained from equation (16) and experimental evaporation data measured at Simcoe in Ontario [*Davies and Allen*, 1973], Konza Prairie [*Sellers et al.*, 1992; *Fritschen*, 1994; *Kanemasu*, 1994], Walnut Creek watershed (Iowa, USA) [*Jackson*, 2003; *Jackson and Cosh*, 2003; *Prueger et al.*, 2009], and Davis, USA [*Katul and Parlange*, 1992]. Based on the reported meteorological data, the parameter b was predicted from equation (20). In addition, the values of E_w and E_p in equation (16) were quantified as $E_R(T_{ss})$ considering the values of T_{ss} (equation (14)) at saturation ($\theta=\theta_{sat}$) and the reported surface water content for each data point, respectively. Hence, surface-atmosphere coupling, central to the CR approach, is embedded in the calculation of E_w and E_p based on meteorological data for the corresponding surface wetness conditions. We provide a worked example in Appendix C to clarify the application of equation (16) for estimating actual evaporation.

The good agreement between experimental data and estimated actual evaporations in Figure 12 represents the usefulness of the complementary relationship for estimating actual evaporation from drying surfaces via prediction of the efficiency parameter (b), and potential and wet surface evaporation rates based on the present model.

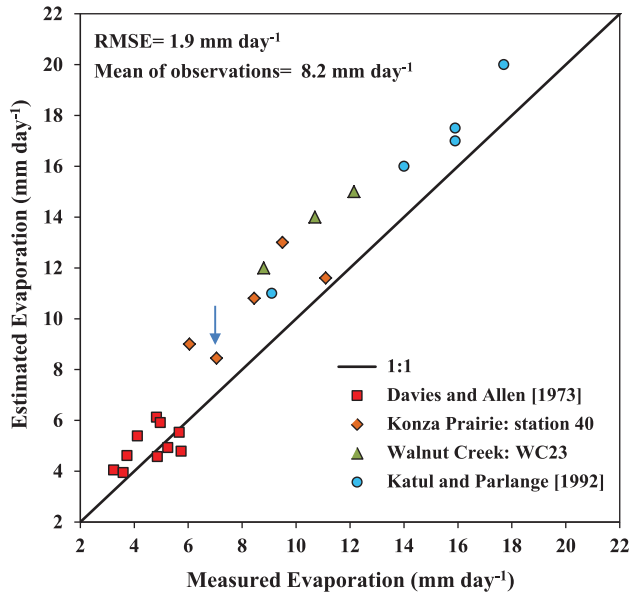

Figure 12. Comparison between estimated actual evaporation (equation (16)) and measured values of actual evaporation using data from four different field experiments: day-light average experimental data of *Davies and Allen* [1973] obtained from measurements in Simcoe, Ontario; Konza Prairie (station 40) [*Sellers et al.*, 1992; *Fritschen*, 1994; *Kanemasu*, 1994]; SMACEX experiments in Walnut Creek (site: WC23) [*Jackson*, 2003; *Jackson and Cosh*, 2003; *Prueger et al.*, 2009], and lysimeter evaporation data of *Katul and Parlange* [1992]. A worked example of the actual evaporation calculation based on equation (16) is presented in Appendix C for the data point marked by the arrow.

6. Summary and Conclusions

We employed a pore-scale representation of evaporation from drying porous surfaces constrained by surface energy balance to define a reference evaporation for steady state conditions with zero sensible heat flux. A unique steady state surface temperature (T_{ss}) that links surface energy balance and evaporation from surfaces at any water content was used to quantify evaporation from a small saturated surface surrounded by drying land surface as the representative of potential evaporation ($E_R(T_{ss})$). The predicted reference evaporation $E_R(T_{ss})$ was in agreement with class A pan evaporation measurements (and with PenPan model predictions) suggesting that the standard class A pan evaporates with minimal sensible heat flux (as also seen in observations of

Lim et al. [2013]). The model was not designed to predict pan evaporation, but instead it enables extension of the asymmetric complementary relationship with analytical prediction of the *b* parameter of *Kahler and Brutsaert* [2006]. The newly derived $E_R(T_{ss})$ and *b* were used in the asymmetric complementary relationship framework to estimate actual evaporation from standard atmospheric measurements yielding good agreement with actual evaporation measurements. The formulation provides insights regarding the meaning of the parameter *b*, supports the broad interpretation of *Granger* [1989] (compare equation (8) with equations (17) and (18)), and links the CR asymmetry to the surface temperature increase as the surface dries and steady state input energy as modulated by the nonlinearity of temperature-vapor pressure relations [*Lintner et al*., 2015].

The concepts presented here, offer a physical framework for quantifying the asymmetric complementary relationship and can be used for prediction of actual evaporation of drying surfaces. The key concept is the recognition that surface temperature (and hence net radiation) changes with variation of surface wetness (wetting or drying) affecting the wet environment evaporation (E_w) and potential evaporation (E_p) in the context of complementary relationship. Hence, the key innovation has been the use of a pore-scale model to explicitly calculate the surface temperature coupled with atmospheric conditions as a function of moisture content and use it to quantify E_w and E_p. Clearly, aspects such as spatial heterogeneity of terrestrial surfaces and meteorological variables, and specific role of vegetation cover must be further investigated to link this pore scale based approach with large scale phenomena of hydrologic and climate interest.

Appendix A: Temporal and Spatial Scales for Steady State Reference Temperature (T_{ss})

Based on the assumption of feedback process between drying land surface and overlying air flow in a closed land atmosphere system (section 3) [*McNaughton*, 1976; *Perrier*, 1980; *Lhomme*,1997] we invoke the following assumptions to resolve the temporal and spatial scales in which the hypothetical steady state condition takes place:

1. Considering the structure of convective boundary layer we focus on the air column below the surface layer (in the CBL that is coupled with the land surface underneath) where vertical fluxes of momentum and heat are almost constant and atmospheric profiles including temperature, wind and moisture profiles change with height significantly [*Driedonks and Tennekes*, 1984; *McNaughton and Spriggs*, 1986; *Metzger et al*., 2007]. Above the surface layer there is a well-mixed layer in which heat, momentum and moisture are thoroughly mixed due to turbulence [*Kaimal et al*., 1976; *Stull*, 1988]. Diurnal growth of the CBL in response to the large-scale vertical velocity or air entrainment from top of the CBL [*Wallace and Hobbs*, 2006] during feedback process between a drying surface and the adjacent air is neglected and for estimating the relevant time scales we assume a constant height for the CBL to facilitate mathematical modeling of the interaction between land and air column below the surface layer. Accordingly, assuming the constant height of ζ for surface layer (5–10% of the CBL height [*Stull*, 1988; *Leclerc and Foken;* 2014]) the volume-averaged temperature (T_{av}) is introduced to represent the temperature of air column below the surface layer.

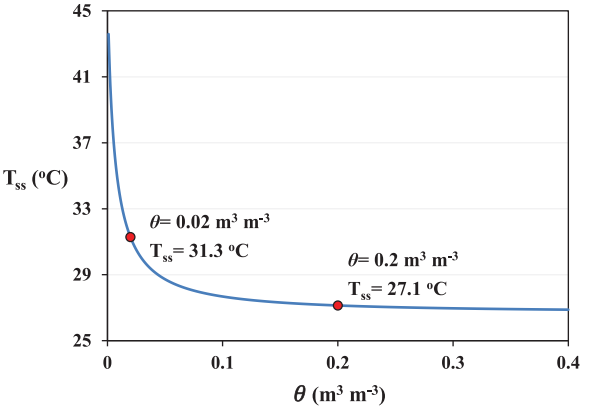

Figure A1. Variation of steady state temperature with surface water content obtained from solution of equation (14) (root finding). U_a=1 m s^{-1}, ε_s=0.9, α=0.2, ε_a=0.8, T_a=25°C and C_a=0.011 kg m^{-3} (rh=50%), $R_{S,net}$=400 W m^{-2}. The symbols mark the value of T_{ss} for two different surface water contents used in Figure A2.

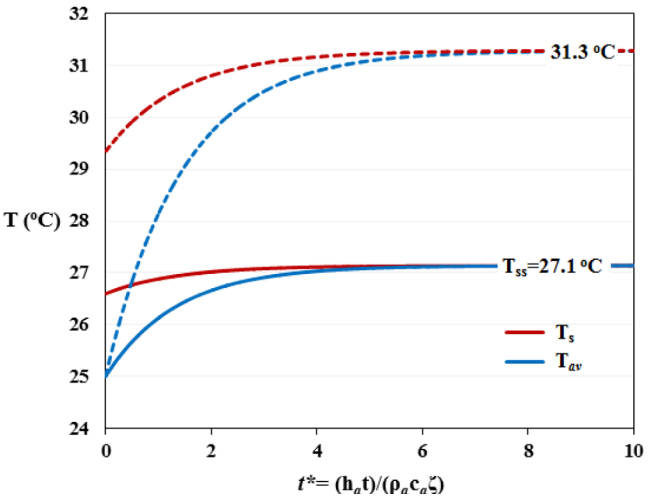

Figure A2. Evolution of soil surface temperature (T_s) and volume-averaged air temperature (T_{av}) obtained from numerical solution of equations (A4) and (A5). The solution was obtained for surface water content of 0.2 $m^3\ m^{-3}$ (solid lines) and 0.02 $m^3\ m^{-3}$ (dashed lines) and same boundary conditions as in Figure A1. The steady state temperature of the system including soil surface with thickness of Δz=1 mm and air column with height of ζ=50 m is same as steady state temperatures in Figure A1 (symbols).

2. Regarding the vertical tekmperature distribution below soil surface we use the assumption of PCEB model [*Aminzadeh and Or*, 2014] in which vertical temperature gradients in the unit cell with thickness of Δz (a single grain size) are neglected. We investigate the energy balance of a surface soil layer with thickness of Δz and temperature of T_s. The Biot number for the soil layer is defined as:

$$Bi=\frac{h_a\,\Delta z}{k} \tag{A1}$$

where h_a is the air thermal convection coefficient and k is thermal conduction coefficient of soil layer. For a range of conditions (e.g., h_a=5−30 W $m^{-2}\ K^{-1}$, k=0.5−2 W $m^{-1}\ K^{-1}$, Δz=0.1−1 mm) the Biot number is of order 10^{-4} to 10^{-2} that is much smaller than 1 and supports the assumption of uniform temperature in a thin soil surface layer.

The unsteady energy balance for the air column with height ζ and soil surface layer with thickness of Δz is written as:

$$\rho_a c_a \zeta \frac{dT_{av}}{dt}=h_a(T_s-T_{av}) \tag{A2}$$

$$\rho_s c_s \Delta z \frac{dT_s}{dt}=(1-\alpha)R_S+\sigma\varepsilon_a T_{av}^4-\sigma\varepsilon_s T_s^4-h_a(T_s-T_{av})-\frac{k}{\Delta Z}(T_s-T_Z)-\frac{D_a\lambda}{\delta(1+\Phi)}[C_{sat}(T_s)-C_a] \tag{A3}$$

in which ρ and c are density and specific heat, respectively. The simultaneous solution of equations (A2) and (A3) leads to the condition in which feedbacks between surface and air temperatures in terms of sensible heat flux and air warming feedbacks result in the thermal equilibrium condition. Temporal discretization of equations (A2) and (A3) is written as:

$$T_{av}^{i+1}=T_{av}^i+\frac{h_a\Delta t}{\rho_a c_a \zeta}(T_s^i-T_{av}^i) \tag{A4}$$

$$T_s^{i+1}=T_s^i+\frac{\Delta t}{\rho_s c_s \Delta z}\left[(1-\alpha)R_S+\sigma\varepsilon_a {T_{av}^i}^4-\sigma\varepsilon_s T_s^{i4}-h_a(T_s^i-T_{av}^i)-\frac{k}{\Delta Z}(T_s^i-T_Z)-\frac{D_a\lambda}{\delta(1+\Phi)}\left[C_{sat}\left(T_s^i\right)-C_a\right]\right] \tag{A5}$$

We then compare steady state temperature of the system including soil surface and air obtained from analytical solution of steady state surface energy balance equation in which zero sensible heat flux reflects the effect of feedback process (equation (14)) with numerical solution of equations (A4) and (A5). Figure A1 depicts the model prediction (equation (14)) of the variation of steady state temperature with surface water content. For the sake of comparison we have plotted evolution of surface and air temperatures for two different surface water contents as 0.2 and 0.02 $m^3\ m^{-3}$ as function of dimensionless time (t^*) (Figure A2) defined as:

$$t^*=\frac{h_a\,t}{\rho_a c_a \zeta} \tag{A6}$$

The system reaches the steady state condition after $t^* \sim 3$ (Figure A2) when both the analytical model (equation (14)) and numerical solution of unsteady energy balance equations (equations (A4) and (A5)) yield the same temperature.

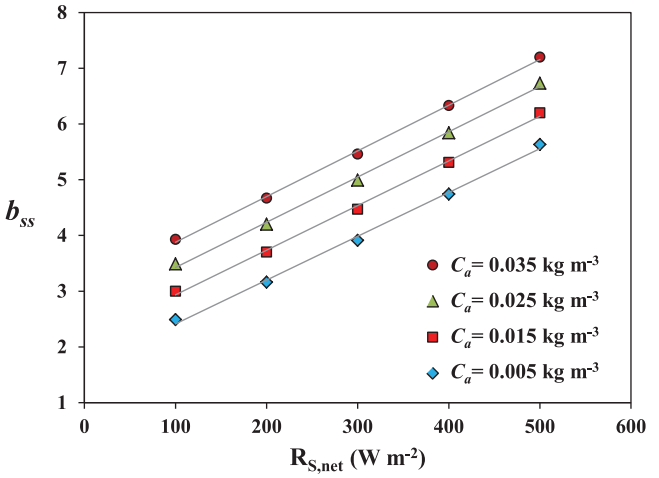

Figure B1. Model predictions of the variation of b_{ss} (equation (19)) versus net shortwave radiation flux for constant wind speed of 2 m s^{-1}.

We invoke the time scale at which the completion of feedback process between overlying air flow and land surface results in a zero sensible heat flux to resolve the spatial scale of the proposed hypothetical steady state condition. Accordingly, the time scale in equation (A6) that was primarily obtained based on vertical transport and mixing processes [*Moene and van Dam*, 2014] between drying land surface and air is used to propose the spatial scale in which the completion of the feedback process takes place. Assuming that spatial heterogeneity of the land surface is negligible, the spatial scale of the expected steady state condition is obtained based on the horizontal distance an air parcel traverses [*Wallace and Hobbs*, 2006] during the feedback process until it reaches the steady state condition as:

$$X = U_a\, t \tag{A7}$$

where X is the surrogate for lateral spatial scale of land-atmosphere exchanges, U_a is the average horizontal wind speed near the surface (e.g., 2 m) and t is the elapsed time since onset of feedback process between land surface and overlying air flow which is obtained from equation (A6). For the mentioned condition in Figures A1 and A2, temporal (t) and spatial (X) scales are quantified as 4.5 hr and 16.5 km, respectively.

Appendix B: Model Prediction of the *b* Parameter for a Range of Conditions

The prediction of the b parameter is based on estimates of the reference evaporation (equation (15)). We use the physically-based model to systematically vary meteorological conditions and estimate the resulting value of the b_{ss} parameter in equation (19). The physical correlation of b_{ss} driven by atmospheric inputs is accordingly denoted as b^*_{ss}. For example, we assume constant wind speed and then calculate b_{ss} for different net shortwave radiation fluxes at constant vapor concentration in the adjacent air mass. Figure B1 shows an example of the variations of b_{ss} versus radiative flux for constant wind speed of 2 m s^{-1} and different vapor concentrations obtained from the current model (equations (15) and (19)). Using the same ranges of vapor concentration and radiation flux, we obtain similar plots for different wind speeds. Assuming linear fitted curves with same slopes, we propose the following expression for estimation of b_{ss}:

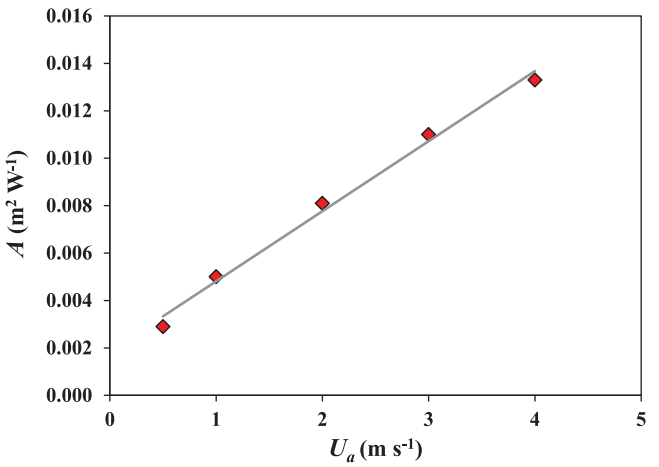

Figure B2. Variation of A in equation (B1) (e.g., the slope of fitted curves in Figure B1 that is related to wind speed of 2 m s^{-1}) versus wind speed. Symbols depict the values obtained from the model and line is the fitted curve.

$$b^*_{ss} = A\, R_{S,net} + B \tag{B1}$$

where $R_{S,net}$ is the net shortwave radiation flux (W m^{-2}) and the

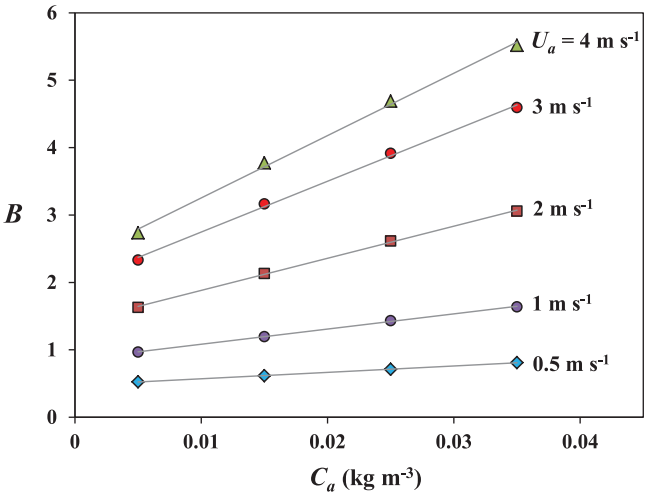

Figure B3. Variation of B (e.g., the intercepts of fitted curves in Figure B1 that is related to wind speed of 2 m s^{-1}) with vapor concentration for different wind speeds.

parameter A (slope of fitted curves) is a function of wind speed (Figure B2):

$$A=(3U_a+2)\times10^{-3} \tag{B2}$$

The parameter B (intercepts of fitted curves in Figure B1) varies for a constant vapor concentration in different plots obtained for different wind speeds. Figure B3 illustrates variation of B with vapor concentration for different wind speeds. Using the interception point of fitted curves in Figure B3 the parameter B can be expressed as:

$$B=(24.3U_a-1.44)(C_a+22.3\times10^{-3})+0.3 \tag{B3}$$

The vapor concentration is also quantified based on air temperature (T_a) and relative humidity (rh) using the Clausius-Clapeyron relationship (assuming air as an ideal gas) as:

$$C_a=611\,rh\frac{M}{RT_a}\exp\left(\frac{\lambda M}{R}\left(\frac{1}{273}-\frac{1}{T_a}\right)\right) \tag{B4}$$

in which M is the water molar mass, R is the universal gas constant, and λ is the latent heat of vaporization.

Appendix C: Worked Example

We provided an example for calculation of actual evaporation using equation (16) for the marked data point in Figure 12. To calculate actual evaporation based on the generalized complementary relationship we need to quantify E_p, E_w, and b. The values of E_w and E_p are obtained from equation (15) considering the value of T_{ss} at saturation ($\theta=\theta_{sat}$) and surface water content of the drying land surface, respectively. Accordingly, equation (14) is employed to calculate $T_{ss}(\theta_{sat})$ and $T_{ss}(\theta)$ and then quantify $E_R(T_{ss}|_{\theta_{sat}})$ and $E_R(T_{ss}|_{\theta})$ in equation (15) as E_w and E_p, respectively. The parameter b is then calculated using equation (20) obtained through the physically based model considering the meteorological conditions including net shortwave radiation flux, wind speed and vapor concentration in the near surface air mass. The associated inputs and calculations are presented in Tables C1 and C2, respectively.

Table C1. Inputs for the Calculation of Actual Evaporation (E_a)

Input	Comments
$R_{S,net}=300$ W m^{-2}	net shortwave radiation flux
$U_a=2.2$ m s^{-1}	mean air velocity
$T_a=25$°C	air temperature
$\theta=0.28$ m^3 m^{-3}	surface water content
$C_a=0.016$ kg m^{-3}	vapor concentration in air
$D_a=2.5\times10^{-5}$ m^2 s^{-1}	vapor diffusion coefficient in air
$v=1.5\times10^{-5}$ m^2 s^{-1}	air kinematic viscosity
$\lambda=2.45$ MJ kg^{-1}	latent heat of water vaporization
$T_Z=23$°C	linearized soil temperature at ΔZ
$\sigma=5.67\times10^{-8}$ W m^{-2} K^{-4}	Stefan-Boltzmann constant
$\varepsilon_a=0.8$	atmospheric emissivity
$\varepsilon_s=0.9$	soil emissivity
$a=150\times10^{-6}$ m	characteristic pore size
$\Phi=0.072$	Schlünder's diffusive resistance parameter in equation (12)
$\delta=0.0015$ m	boundary layer thickness ($\frac{22v}{0.1U_a}$)

Table C2. Calculations for Actual Evaporation (E_a)

Parameter	Calculation
$T_{ss}\|_{\theta_{sat}}$=24.75°C	Equation (14)
$T_{ss}\|_{\theta=0.28}$=24.9°C	Equation (14)
$E_R(T_{ss}\|_{\theta_{sat}})$=8.5 mm day^{-1}	Equation (15) (E_w in Equation 16)
$E_R(T_{ss}\|_{\theta=0.28})$=8.8 mm day^{-1}	Equation (15) (E_p in Equation 16)
b^*_{ss}=4.9	Equation (20) (b in Equation 16)
E_a =8.45 mm day^{-1}	Equation (16)

Nomenclature

A	Coefficient in equation (20) (m^2 W^{-1})
a	Characteristic pore size (m)
B	Coefficient in equation (20)
Bi	Biot number $(\frac{h_a \Delta z}{k})$
b	Empirical constant $(\frac{E_p - E_w}{E_w - E_a})$
b_{ss}	Physically based prediction of b
b^*_{ss}	Correlation-based estimate of b_{ss} driven by atmospheric conditions
C_a	Vapor concentration in air (kg m^{-3})
C_{sat}	Saturated vapor concentration (kg m^{-3})
c_a	Specific heat of air (J kg^{-1} K^{-1})
c_s	Specific heat of soil (J kg^{-1} K^{-1})
D_a	Vapor diffusion coefficient in air (m^2 s^{-1})
DPA	Drying power of air (W m^{-2})
E_a	Actual evaporation (mm day^{-1})
E_{a+}	Scaled actual evaporation $(\frac{E_a}{E_w})$
E_{MI}	Dimensionless moisture index $(\frac{E_a}{E_p})$
E_p	Potential evaporation (mm day^{-1})
E_{pan}	Pan evaporation (mm day^{-1})
E_{p+}	Scaled potential evaporation $(\frac{E_p}{E_w})$
E_R	Steady state reference evaporation (mm day^{-1})
E_w	Wet environment evaporation (mm day^{-1})
e_a	Air vapor pressure (Pa)
e^*_p	Saturated vapor pressure at surface temperature (T_s) (Pa)
e_s	Vapor pressure at drying surface (Pa)
e^*_w	Saturated vapor pressure at T_w (Pa)
G	Soil heat flux (W m^{-2})
H	Sensible heat flux (W m^{-2})
h_a	Air thermal convection coefficient (W m^{-2} K^{-1})
k	Effective thermal conductivity of soil (W m^{-1} K^{-1})
L	Conversion coefficient ($\rho_w.\lambda$) (J m^{-3})
LE	Latent heat flux (W m^{-2})
LE_{Pe}	*Penman*'s [1948] equation for potential evaporation (W m^{-2})
LE_{P-T}	*Priestley and Taylor*'s [1972] estimation of potential evaporation (W m^{-2})
M	Water molar mass (kg mol^{-1})
R	Molar gas constant (8.314 J mol^{-1} K^{-1})
$R_{L,in}$	Incoming long wave radiation (W m^{-2})
$R_{L,out}$	Outgoing long wave radiation (W m^{-2})
R_n	Net radiation flux (W m^{-2})
R_S	Incoming shortwave radiation flux (W m^{-2})
$R_{S,net}$	Net shortwave radiation flux $((1-\alpha)R_S)$ (W m^{-2})
rh	Relative humidity (%)
T_a	Air temperature (K)
T_{av}	Average air temperature in surface layer (K)

T_s	Soil surface temperature (K)
T_{ss}	Steady state temperature (K)
T_w	Wet surface temperature (K)
T_Z	Linearized soil temperature at ΔZ (K)
t^*	Dimensionless time $(\frac{h_a t}{\rho_a c_{a\zeta}})$
t	Temporal scale (s)
U_a	Mean air velocity (m s^{-1})
X	Spatial scale (m)
α	Surface albedo for shortwave radiation
α_{P-T}	Priestley-Taylor coefficient
ε_a	Atmospheric emissivity
ε_s	Soil emissivity
Δ	Slope of saturated vapor pressure-temperature curve (Pa K^{-1})
Δ^*	Slope of vapor pressure-temperature curve in *Granger* [1989] (Pa K^{-1})
ΔZ	Thermal decay depth below the surface (m)
Δz	Thickness of soil surface layer (m)
δ	Boundary layer thickness $(\frac{22\nu}{0.1U_a})$ (m)
ζ	Height of surface layer (m)
γ	Psychrometric constant (Pa K^{-1})
λ	Latent heat of water vaporization (J kg^{-1})
θ	Surface water content (m^3 m^{-3})
ν	Air kinematic viscosity (m^2 s^{-1})
ρ_a	Air density (kg m^{-3})
ρ_s	Soil density (kg m^{-3})
ρ_w	Water (liquid) density (kg m^{-3})
Φ	Schlünder's diffusive resistance parameter in equation (12)
σ	Stefan-Boltzmann constant (5.67×10^{-8} W m^{-2} K^{-4})

Acknowledgments

Data supporting the results of this study are available upon request from corresponding author (milad.aminzadeh@usys.ethz.ch). The authors gratefully acknowledge funding by the Swiss National Science Foundation (200021-113442), and support for a visit to the Australian Research Council Centre of Excellence for Climate Systems Science at the ANU and UNSW (D.O.). The manuscript benefitted greatly from numerous discussions with Stanislaus Schymanski (ETH Zürich), and the many insightful review comments of Guido Salvucci (Boston University), Benjamin Lintner (Rutgers University), and Tim McVicar (CSIRO Land and Water).

References

Aminzadeh, M., and D. Or (2013), Temperature dynamics during nonisothermal evaporation from drying porous surfaces, *Water Resour. Res.*, *49*, 7339–7349, doi:10.1002/2013WR014384.

Aminzadeh, M., and D. Or (2014), Energy partitioning dynamics of drying terrestrial surfaces, *J. Hydrol.*, *519*, 1257–1270.

Bateni, S. M., and D. Entekhabi (2012), Relative efficiency of land surface energy balance components, *Water Resour. Res.*, *48*, W04510, doi:10.1029/2011WR011357.

Bouchet, R. J. (1963), Evapotranspiration reelle, evapotranspiration potentielle, et production agricole, *Ann. Agron.*, *14*, 543–824.

Brutsaert, W. (2005), *Hydrology: An Introduction*, Cambridge Univ. Press, N. Y.

Brutsaert, W., and M. B. Parlange (1998), Hydrologic cycle explains the evaporation paradox, *Nature*, *396*, 30.

Brutsaert, W., and H. Stricker (1979), An advection-aridity approach to estimate actual evapotranspiration, *Water Resour. Res.*, *15*, 443–450.

Crago, R., and R. Crowley (2005), Complementary relationships for near instantaneous evaporation, *J. Hydrol.*, *300*, 199– 211.

Davies, J. A., and C. D. Allen (1973), Equilibrium, potential and actual evaporation from cropped surfaces in Southern Ontario, *J. Appl. Meteorol.*, *12*, 649–657.

Donohue, R. J., T. R. McVicar, and M. L. Roderick (2010), Assessing the ability of potential evaporation formulations to capture the dynamics in evaporative demand within a changing climate, *J. Hydrol.*, *386*(1-4), 186–197, doi:10.1016/j.jhydrol.2010.03.020.

Driedonks, A. G. M., and H. Tennekes (1984), Entrainment effects in the well-mixed atmospheric boundary layer, *Boundary Layer Meteorol.*, *30*, 75–105.

Edinger, J. E., D. W. Duttweiller, and J. C. Geyer (1968), The response of water temperature to meteorological conditions, *Water Resour. Res.*, *4*, 1137–1143.

Environment Canada (2014). [Available at http://climate.weather.gc.ca/advanceSearch/searchHistoricData_e.html, last accessed 5 Aug. 2014.]

Fritschen, L. J. (1994), Bowen Ratio Surf[ace]. Flux: Fritschen (FIFE). Oak Ridge Natl. Lab. Distrib. Active Arch. Cent., Oak Ridge, Tenn., doi:10.3334/ORNLDAAC/19. [Available at http://www.daac.ornl.gov.]

Granger, R. J. (1989), A complementary relationship approach for evaporation from non-saturated surfaces, *J. Hydrol.*, *111*, 31–38.

Haghighi, E., and D. Or (2013), Evaporation from porous surfaces into turbulent airflows: Coupling eddy characteristics with pore scale vapor diffusion, *Water Resour. Res.*, *49*, 8432–8442, doi:10.1002/2012WR013324.

Haghighi, E., and D. Or (2015), Interactions of bluff-body obstacles with turbulent airflows affecting evaporative fluxes from porous surfaces, *J. Hydrol.*, *530*, 103–116.

Haghighi, E., E. Shahraeeni, P. Lehmann, and D. Or (2013), Evaporation rates across a convective air boundary layer are dominated by diffusion, *Water Resour. Res.*, *49*, 1602–1610, doi:10.1002/wrcr.20166.

Hisatake, K., M. Fukuda, J. Kimura, M. Maeda, and Y. Fukuda (1995), Experimental and theoretical study of evaporation of water in a vessel, *J. Appl. Phys.*, *77*, 6664–6674, doi:10.1063/1.359079.

Hobbins, M. T., J. A. Ramirez, T. C. Brown, and L. Claessens (2001), The complementary relationship in estimation of regional evapotranspiration: The complementary relationship areal evapotranspiration and advection-aridity models, *Water Resour. Res.*, *37*, 1367–1387.

Jackson, T. (2003), *SMEX02 Watershed Soil Moisture Data, Walnut Creek, Iowa*, NASA Natl. Snow and Ice Data Cent. Distrib. Active Arch. Cent., Boulder, Colo., doi:10.5067/OAO4SU0XZLGR.
Jackson, T., and M. Cosh (2003), *SMEX02 Tower-Based Radiometric Surface Temperature, Walnut Creek, Iowa*, NASA Natl. Snow and Ice Data Cent. Distrib. Active Arch. Cent., Boulder, Colo., doi:10.5067/BJZU6IV9HUTE.
Jensen, M. E., and H. R. Haise (1963), Estimating evaporation from solar radiation, *J. Irrig. Drain. Div. Am. Soc. Civ. Eng.*, *89*, 15–41.
Kahler, D. M., and W. Brutsaert (2006), Complementary relationship between daily evaporation in the environment and pan evaporation, *Water Resour. Res.*, *42*, W05413, doi:10.1029/2005WR004541.
Kaimal, J. C., D. A. Haugen, O. R. Cote, Y. Izumi, S. J. Caughey, and C. J. Readings (1976), Turbulence structure in the convective boundary layer, *J. Atmos. Sci.*, *33*, 2152–2169.
Kanemasu, E. T. (1994), Soil Moisture Neutron Probe Data (FIFE), Oak Ridge Natl. Lab. Distrib. Active Arch. Cent., Oak Ridge, Tenn., doi: 10.3334/ORNLDAAC/111. [Available at http://www.daac.ornl.gov.]
Katul, G. G., and M. B. Parlange (1992), A Penman-Brutsaert Model for wet surface evaporation, *Water Resour. Res.*, *28*, 121–126, doi: 10.1029/91WR02324.
Leclerc, M. Y., and T. Foken (2014), *Footprints in Micrometeorology and Ecology*, Springer, Berlin, doi:10.1007/978-3-642-54545-0_1.
Lhomme, J. P. (1997), A theoretical basis for the Priestley-Taylor coefficient, *Boundary Layer Meteorol.*, *82*, 179–191.
Lim, W. H., M. L. Roderick, M. T. Hobbins, S. C. Wong, P. J. Groeneveld, F. Sun, and G. D. Farquhar (2012), The aerodynamics of pan evaporation, *Agric. For. Meteorol.*, *152*, 31–43, doi:10.1016/j.agrformet.2011.08.006.
Lim, W. H., M. L. Roderick, M. T. Hobbins, S. C. Wong, and G. D. Farquhar (2013), The energy balance of a US Class A evaporation pan, *Agric. For. Meteorol.*, *182–183*, 314–331, doi:10.1016/j.agrformet.2013.07.001.
Linacre, E. T. (1994), Estimating U.S. class A pan evaporation from few climate data, *Water Int.*, *19*, 5– 14.
Lintner, B. R., P. Gentine, K. L. Findell, and G. D. Salvucci (2015), The Budyko and complementary relationships in an idealized model of large-scale land-atmosphere coupling, *Hydrol. Earth Syst. Sci.*, *19*, 2119–2131, doi:10.5194/hess-19-2119-2015.
Machin, J. (1970), The study of evaporation from small surfaces by the direct measurement of water vapour pressure gradients, *J. Exp. Biol.*, *53*, 753–762.
McMahon, T. A., M. C. Peel, L. Lowe, R. Srikanthan, and T. R. McVicar (2013), Estimating actual, potential, reference crop and pan evaporation using standard meteorological data: A pragmatic synthesis, *Hydrol. Earth Syst. Sci.*, *17*, 1331–1363.
McNaughton, K. G. (1976), Evaporation and advection I: Evaporation from extensive homogeneous surfaces, *Q. J. R. Meteorol. Soc.*, *102*, 181–191.
McNaughton, K. G., and T. W. Spriggs (1986), A mixed-layer model for regional evaporation, *Boundary Layer Meteorol.*, *34*, 243–262.
McNaughton, K. G., and T. W. Spriggs (1989), An evaluation of the Priestley and Taylor equation and the complementary relationship using results from a mixed-layer model of the convective boundary layer, in *Estimation of Aerial Evapotranspiration*, edited T. A. Black et al., pp. 89–104, Int. Assoc. of Hydrol. Sci., Wallingford, U. K.
Metzger, M., B. J. McKeon, and H. Holmes (2007), The near-neutral atmospheric surface layer: Turbulence and non-stationarity, *Philos. Trans. R. Soc. A*, *365*, 859, doi:10.1098/rsta.2006.1946.
Milly, P. C. D., and K. A. Dunne (2011), On the hydrologic adjustment of climate-model projections: The potential pitfalls of potential evapotranspiration, *Earth Interact.*, *15*, 1–14, doi:10.1175/2010ei363.1.
Moene, A. F., and J. C. van Dam (2014), *Transport in the Atmosphere-Vegetation-Soil Continuum*, Cambridge Univ. Press, New York.
Monteith, J. L. (1965), Evaporation and environment, *Symp. Soc. Exp. Biol.*, *19*, 205–234.
Monteith, J. L. (1981), Evaporation and surface temperature, *Q. J. R. Meteorol. Soc.*, *107*, 1–27.
Morton, F. I. (1983), Operational estimates of areal evapotranspiration and their significance to the science and practice of hydrology, *J. Hydrol.*, *66*, 1–76.
Morton, F. I. (1991), A discussion of four papers on evaporation in volume 111, *J. Hydrol.*, *124*(3-4), 363–374.
Nash, J. E. (1989), Potential evaporation and "the complementary relationship," *J. Hydrol.*, *111*, 1–7.
Penman, H. L. (1948), Natural evaporation from open water, bare soil, and grass, *Proc. R. Soc. London, Ser. A*, *193*, 120–146.
Perrier, A. (1980), *Etude Microclimatique des Relations Entre les Proprietes de Surface et les Caracteristiques de l'Air*, Meteorol. et Environnement, Evry, France.
Pettijohn, J. C., and G. D. Salvucci (2009), A new two-dimensional physical basis for the complementary relation between terrestrial and pan evaporation, *J. Hydrometeorol.*, *10*(2), 565–574, doi:10.1175/2008JHM1026.1.
Priestley, C. H. B., and R. J. Taylor (1972), On the assessment of surface heat flux and evaporation using large-scale parameters, *Mon. Weather Rev.*, *100*(2), 81–92.
Prueger, J., J. Hatfield, J. Albertson, T. Cahill, D. Cooper, B. Eichinger, L. Hipps, B. Kustas, and J. Norman (2009), *SMEX02 SMACEX Tower Meteorological/Flux Data: Iowa*, NASA DAAC, Natl. Snow and Ice Data Cent., Boulder, Colo.
Raupach, M. R. (2001), Combination theory and equilibrium evaporation, *Q. J. R. Meteorol. Soc.*, *127*, 1149–1181.
Roderick, M. L., L. D. Rotstayn, G. D. Farquhar, and M. T. Hobbins (2007), On the attribution of changing pan evaporation, *Geophys. Res. Lett.*, *34*, L17403, doi:10.1029/2007GL031166.
Rotstayn, L. D., M. L. Roderick, and G. D. Farquhar (2006), A simple pan-evaporation model for analysis of climate simulations: Evaluation over Australia, *Geophys. Res. Lett.*, *33*, L17715, doi:10.1029/2006GL027114.
Schlünder, E. U. (1988), On the mechanism of the constant drying rate period and its relevance to diffusion controlled catalytic gas phase reactions, *Chem. Eng. Sci.*, *43*(10), 2685–2688, doi:10.1016/0009-2509(88)80012-5.
Sellers, P. J., F. J. Hall, G. Asrar, D. E. Strebel, and R. E. Murphy (1992), An overview of the First International Satellite Land Surface Climatology Project (ISLSCP) Field Experiment (FIFE), *J. Geophys. Res.*, *97*, 18,345–18,371.
Shahraeeni, E., and D. Or (2011), Quantification of subsurface thermal regimes beneath evaporating porous surfaces, *Int. J. Heat Mass Transfer*, *54*, 4193–4202, doi:10.1016/j.ijheatmasstransfer.2011.05.024.
Shahraeeni, E., P. Lehmann, and D. Or (2012), Coupling of evaporative fluxes from drying porous surfaces with air boundary layer–Characteristics of evaporation from discrete pores, *Water Resour. Res.*, *48*, W09525, doi:10.1029/2012WR011857.
Shuttleworth, W. J. (2012), *Terrestrial Hydrometeorology*, John Wiley, West Sussex, U. K., doi:10.1002/9781119951933.
Shuttleworth, W. J. (2014), Interactive comment on "Technical Note: On the Matt–Shuttleworth approach to estimate crop water requirements" by J. P. Lhomme et al., Hydrol. Earth Syst. Sci. Discuss., 11, C1186–C1188.
Shuttleworth, W. J., A. Serrat-Capdevila, M. L. Roderick, and R. L. Scott (2009), On the theory relating changes in area-average and pan evaporation, *Q. J. R. Meteorol. Soc.*, *135*, 1230–1247, doi:10.1002/qj.434.
Slatyer, R. O., and I. C. McIlroy (1961), *Practical Microclimatology*, Commonwealth Scientific and Industrial Research Organisation (CSIRO), Melbourne, Australia.

Stull, R. B. (1988), *An Introduction to Boundary Layer Meteorology*, Kluwer Academic Publishers, Dordrecht.
Szilagyi, J. (2007), On the inherent asymmetric nature of the complementary relationship of evaporation, *Geophys. Res. Lett.*, *34*, L02405, doi:10.1029/2006GL028708.
Thom, A. S., J. L. Thony, and M. Vauclin (1981), On the proper employment of evaporation pans and atmometers in estimating potential transpiration, *Q. J. R. Meteorol. Soc.*, *107*, 711–736.
Venturini, V., C. Krepper and L. Rodriguez (2012), Evapotranspiration estimation based on the complementary relationships, in *Evapotranspiration––Remote Sensing and Modeling*, edited by A. Irmak, pp. 19–40, InTech, Rijeka.
Wallace, J. M., and P. V. Hobbs (2006), *Atmospheric Science: An Introductory Survey*, 2nd ed., Academic Press, N. Y.
Western Regional Climate Center (2014). [Available at http://www.wrcc.dri.edu/htmlfiles/westevap.final.html, last accessed 5 Oct. 2014.]
Yang, Y., H. Su, R. Zhang, and J. Xia (2013), Revised advection-aridity evaporation model, *J. Hydrol. Eng.*, *18*(6), 655–664.